JMEPEG (2022) 31:5523–5534
https://doi.org/10.1007/s11665-022-06614-w

1059-9495/$19.00

TECHNICAL ARTICLE

Synergistic Effect of Amino-Functionalized Multiwalled Carbon Nanotube Incorporated Polyurethane Nanocomposites for High-Performance Smart Materials Applications

Naveed Ahmed, Fatima Iftikhar, Usman Farooq, Basit Niaz, Saad Nauman, Nisar Ahmed, Muhammad Arsalan Dilbraiz, and Saad Ahmed

Submitted: 22 March 2021 / Revised: 20 October 2021 / Accepted: 28 November 2021 / Published online: 8 March 2022

In the present study, thermoplastic polyurethane (PU) and its nanocomposites have been synthesized using a chain-growth process without a catalyst. The mixture of dual-functionalized multiwalled carbon nanotubes (FMWCNTs) (amino and acid functionalized) was used to enhance chemical and physical interlinking between carbon filler and PU matrix in nanocomposites. The structure of pre-designed synthesized PU and its nanocomposites were confirmed by Fourier transformed infrared analysis, and the degree of crystallinity was analyzed by x-ray diffraction analysis. Scanning electron microscopy morphologies confirm better interfacial interaction between dual-FMWCNTs and PU matrix with very little aggregation at higher loading amount of filler content. Excellent improved thermal stabilities with increase loading amount of functionalized filler were confirmed by thermal gravimetric analysis (TGA). A significant increase in mechanical property of PU-nanocomposites with 3% filler loading was observed 62.4 MPa relative to 32.4 MPa of neat-PU, respectively. The shape recovery (SR) time of thermally triggered nanocomposites was improved significantly due to the better thermal conduction of dual-FMWCNTs. A prompt fast recovery response in less than 10 seconds was recorded for the nanocomposite sample. According to our best knowledge, a fast recovery time of fewer than 10 seconds will be a good approach for high material smart applications which is not reported till somewhere else.

Keywords chemical interaction, dual-FMWCNTs, polyurethane, thermally induced shape recovery

1. Introduction

Smart polymers are materials that can change the structure and physical properties in response to external stimuli. Shape memory polymers (SMP) can regain their novel shape from a provisionally distorted state upon responding to an exterior stimulus such as temperature, chemical, light, electrical or electromagnetic field (Ref 1-4). SMP was enviable for electrical cabling safety due to their mutual insulation, anti-corrosion, mechanical shield, and damage relief in the past. Prominent advances in the SMP field have taken place in current years which have altered the predictable view of SMPs and led to further prospects for higher advanced applications such as aerospace, bio-medical, textile, and industrial. Attaining shape memory (SM) properties in a polymer normally involve the generation of networks via physical or chemical cross-linking reactions in the polymer (Ref 5-11).

Despite the huge range of possible shapes that can be created, the SMP has a major disadvantage in terms of hardness and mechanical or tensile strength. Additional key limitation includes very modest thermal conductivity, electrical inertness, electromagnetic and slow response and large recovery time to light, heat and chemical stimuli through actuation. Probable applications of these kinds of materials are often insufficient when high-performance is necessary. A novel class of shape memory nanocomposites (SMC) has been proposed to address these issues (Ref 12-17).

Polyurethane (PU) belongs to the most significant group of polymers that established immense attention in several applications, ranging from industrial (e.g., adhesives, coating, and textiles) to bio-medical (e.g., drug delivery and tissue engineering) (Ref 18-21). These kinds of polymers are based on alternating soft segment domains (normally aliphatic polyether and polyesters) and hard segments consist of (aromatic urethanes), which produce phase separation because of segmental incompatibility. PU is a versatile engineering substance due to its excellent flexibility and elasticity (Ref 22). As mechanical properties are concerned, alter in the polymer chain backbone can fetch important modifications in the mechanical properties like tensile strength (Ref 23, 24). An increase in urethane linkage number carries a considerable increase in the hydrogen bonding which advances the tensile properties of these polymers (Ref 25-27).

Naveed Ahmed, Fatima Iftikhar, Basit Niaz, and **Muhammad Arsalan Dilbraiz**, Department of Chemistry, Hazara University, Mansehra 21300 Khyber Pukhtunkhwa, Pakistan; **Usman Farooq** and **Saad Ahmed**, Department of Chemistry, University of Okara, Okara, Pakistan; **Saad Nauman** and **Nisar Ahmed**, Department of Material science and engineering, Institute of space technology (IST), Islamabad, Pakistan. Contact e-mail: saadahmed@uo.edu.pk.

Carbon nanotubes (CNTs) are tiny hollow tubes having a diameter of 0.4∼2.5 nm. The exceptional features of CNTs tender capacity for fabrication in polymer composites with significantly superior improved properties like strength, excellent conductivity, super elasticity, superior durability, excellent shape recovery, enhanced thermal stability, and toughness. CNTsreinforced polymer composites have captivated much attention because of the enhanced compatibility of nanofiller and polymer (Ref 28-31). The CNTs addition for reinforcement enhances the PUs nanocomposite's hardness, tensile strength, compressive strength, elastic modulus, toughness, thermal conductivity as well as thermal stabilities (Ref 32-35).

In this research, we developed an excellent way of uniform dispersion of nanofiller in the polymer matrix by grafting with two different functional groups. PU was prepared in catalyst free environment by the reaction of toluene diisocyanate (TDI) with polyethylene glycol (PEG), and phloroglucinol (PGC) was used as chain extender by adjusting their ratios to control over hard and soft domains for enhanced properties attainment. The solution mixing approach was used for nanofiller fabrication in polymer matrix because of its advantage over ordinary techniques, and it helps in uniform dispersion of nanofiller in polymer matrix by avoiding aggregates formation which leave weak spot and causes low tensile strength and shape recovery properties and repeatability. Amino-FMWCNTs and acid-FMWCNTs were prepared and their (1:1) mixture was used to generate physical and chemical interaction between filler and PU matrix. The incorporation of hybrid filler system in polymer matrix system provides excellent thermal stabilities, tensile strength and conductive properties to system which help in efficient and repeatable shape recoveries as well as provide robustness to the system without any significant change in physical and chemical properties. A series of PU/dual-FMWCNTs nanocomposites was synthesized and their mechanical, thermal, and shape memory properties were compared for future smart materials application on a larger scale.

2. Experimental Section

2.1 Materials and Methods

Polyethylene glycol (PEG) average molecular weight (Mn∼4000), tetrahydrofuran (THF) 99.5%, stannous chloride ($SnCl_2$), multiwall carbon nanotubes (MWCNTs) having obtained diameter and length (O.D._L) 6-9nm 95% (carbon) were used as received from Sigma (UK). Toluene diisocyanate (TDI) 97%, sulfuric acid (H_2SO_4), nitric acid (HNO_3), phloroglucinol (PGC), and hydrochloric acid (HCl) were obtained from Sigma (UK)

2.2 MWCNTs Functionalization

2.2.1 Acid-Functionalization of MWCNTs. Firstly, 2-grams of multiwalled carbon nanotube (MWCNT) having dimensions O.D._L 6∼9 nm_5 mm, respectively, and >95% (carbon) were first sonicated. MWCNTs were refluxed in a mixture of 5 M nitric acid (HNO_3) and 8 M sulfuric acid (H_2SO_4) (1:3) for 24 hours at 70 °C. Filtration was performed with cellular membrane filter paper with deionized water. Numerous washes with deionized water were performed to attain pH around (6∼7) for acid-functionalized MWCNTs as described in our previous work (Ref 36).

2.2.2 Amino-Functionalization of MWCNTs. After purification, of 3 g of MWCNTs were dissolved in 30 ml of THF by constant stirring. A mixture of HNO_3 and H_2SO_4 of (70:30) ratios was prepared. Slow addition of acidic mixture in MWCNTs solution was performed using an ice bath. After complete addition with constant stirring, the resulting mixture was neutralized with NaOH solution. Several washes with distilled water were performed for complete neutralization. After filtration, the nitro-functionalized MWCNTs were dried for 8∼10 hours in the oven.

A 2 g of nitro-functionalized MWCNTs was taken and dissolved in 20 ml of THF. The mixture of 10 g of $SnCl_2$ and 20 ml of HCl was taken and heated at 60 °C until a complete color change. Both solutions were mixed thoroughly in a round bottom flask and put under reflux at 80 °C for 2 hours. After that solution was washed with NaOH solution to neutralize and after several washes, with distilled water, the amino-functionalized MWCNTs were obtained and dried at 60 °C for 10 hours (Ref 37).

2.3 Synthesis of Polyurethane with a Chain Extender

TDI (97%) 0.8 g and polyethylene glycol (M.W ∼ 4000) 0.7 g were dissolved in tetrahydrofuran (THF) 95% to obtain polyurethane pre-polymer (PU pre-polymer) by a condensation reaction. The solution was refluxed at 80°C for 3∼4 hours with steady stirring to gain pre-polymer. After pre-polymer synthesis, PGC 0.4 g was further added as a chain extender to obtain segmented-PU. The resulting segmented-PU was transferred into petri dish for casting film at ambient temperature.

2.4 Synthesis of Polyurethane Composite with Functionalized MWCNTs (FMWCNTs)

For polyurethane nanocomposite (PUNC) synthesis, the same method was adopted as discussed in the previous section. The mixture of amino-functionalized multiwall carbon nanotubes (amino-FMWCNTs) and acid-functionalized multi-walled carbon nanotubes (acid-FMWCNTs) (1:1) was dissolved into 20 ml of THF. The resulting solution was added to the entire mixture and let to reflux for the next 2 to 3 hours. The sonication was done for the next 1∼2 hour. The mixture was transferred into petri dish for film casting at room temperature (Table 1).

2.5 Characterization Techniques

2.5.1 Fourier Transform Infrared Spectroscopy (FTIR). FTIR spectrum of the samples was performed to confirm the structure of pre-designed PU and its blends using Model No FT/IR-6600 manufactured by JASCO type.

2.5.2 Thermal Gravimetric Analysis (TGA). For TGA analysis, SDT-60 apparatus loaded with TGA/HT DSC HSS2 was used manufactured in (Japan). The comparison of thermal stabilities of the sample was performed. The percentage loss of the sample was determined with an increase in temperature from 0 to 700 °C at a constant raging rate of 10 °C/min.

2.5.3 Scanning Electron Microscopy (SEM). Tescan Orsay Holding Mira-3 TESCAN made in (Czech Republic) was used for FE-SEM study to see the change in surface morphologies of PU and its blends. A thick gold coating was used for the samples using a gold sputter coating machine before preceding to SEM study.

2.5.4 Mechanical Test. A universal testing machine (Instron 5565) with a strain rate of 5 mm/min at 25 °C was used for stress-strain performance analysis according to ASTM D638 standard method. Before tensile analysis, sample was cut into a dog-bone shape before performing the test (Fig. 1 and 2).

2.5.5 X-ray Diffraction Analysis (XRD). X-ray analysis of the sample was performed to study the degree of crystallinity and amorphous nature of the polymer and its blends with MWCNTs. XRD studies were proceeded by using the Theta-Theta diffractometer made by STOE (Germany).

2.5.6 The Thermo-Responsive Shape Memory Effect. For the thermo-responsive shape memory effect, the indirect heating source was used in a particularly built setup. Indirect heating was applied to avoid the combustion of polymer because direct heating can damage polymer. The equipment consists of a hot plate having a petri dish, thermometer. The sample was cut into the desired strip and then the temperature of the hotplate was raised to 80 °C. The sample was placed on a petri dish for heating after maintaining the temperature. Followed by heating, the sample was removed and deformed by using physical load before proper cooling. After deformation, sample was placed at ambient temperature for cooling to fix into a deformed shape. The sample was replaced in a petri dish after cooling at room temperature, and the shape recovery over time was documented. Furthermore, using a typical Vernier caliper, the percentage shape recovery was calculated as follows:

$$\mathrm{SR} = \frac{l_R}{l_D} \times 100$$

SR = Percentage shape recovery, l_d = Length of total deformed shape, l_R = Length of recovered shape

Table 1 Sample codes and composition of synthesized thin films

Sample code	TD1/PEG/PGC/dual-FMWCNTs	Composition
P-control	0.8/0.7/0.4/-	Neat-polyurethane
P-CA1	0.8/0.7/0.4/-0.01g	Polyurethane/0.01g dual-FMWCNTs
P-CA2	0.8/0.7/0.4/0.05g	Polyurethane/0.05g dual-MWCNTs
P-CA3	0.8/0.7/0.4/0.1g	Polyurethane/0.1g dual-FMWCNTs
P-CA4	0.8/0.7/0.4/0.3g	Polyurethane/0.3g dual-FMWCNTs
P-CA5	0.8/0.7/0.4/0.5g	Polyurethane/0.5g dual- FMWCNTs
P-CA6	0.8/0.7/0.4/0.7g	Polyurethane/0.7g dual-FMWCNTs

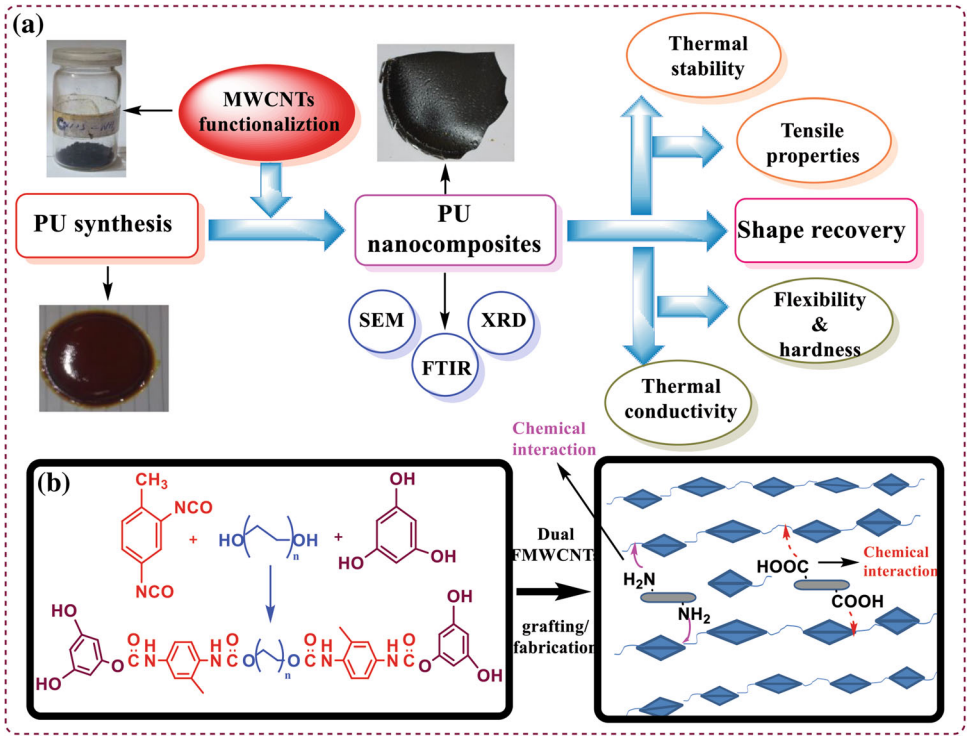

Fig. 1 (a). Schematic synthesis flowchart, (b). Structure of synthesized neat-PU and its architecture in nanocomposite

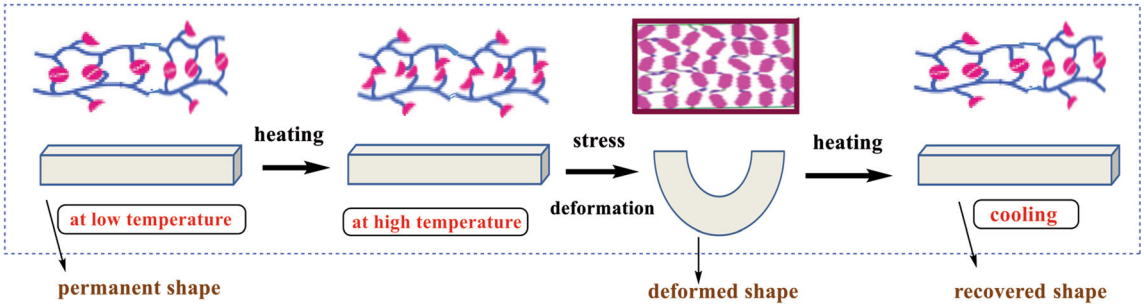

Fig. 2 Complete shape recovery phenomenon with molecular architecture for synthesized PU thin films

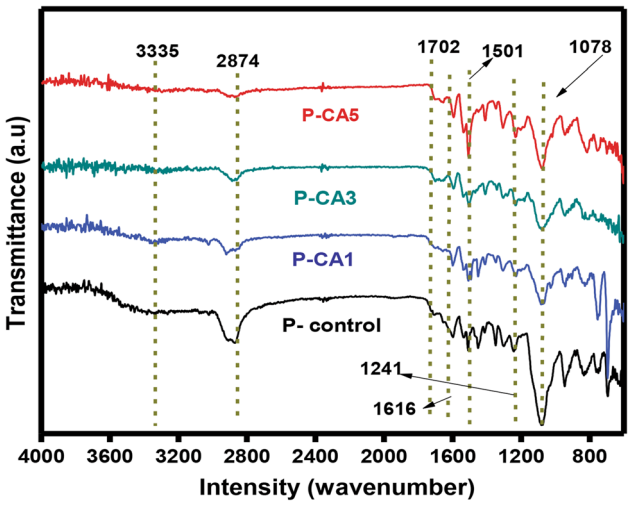

Fig. 3 FTIR spectra of samples selected samples (P-control, P-CA1, P-CA3, and P-CA5)

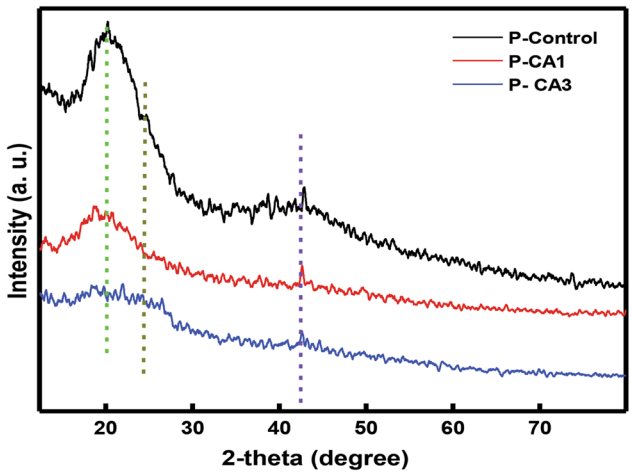

Fig. 4 XRD spectra of selected samples sample (P-control, P-CA1, and PCA3)

3. Results and Discussion

3.1 FTIR Analysis

The N-H stretching absorbance peak for the characteristic band of polyurethane can be seen in Fig. 3 in the FTIR spectrum of the sample, which is around 3335-3400 cm^{-1}. NCO peak disappearance around 2200∼2250 cm^{-1} and appearance of a peak at 3400 cm^{-1} are involved in the pre-designed polyurethane synthesis (Ref 38). The peak around 2874∼2922 cm^{-1} reveals the CH- symmetric stretching vibrations of the CH_2 group. The characteristic absorbance peak around 1702∼1722 cm^{-1} represents urethane-free non-hydrogen bonded C=O, similarly, the absorbance peak of symmetric stretching vibrations at 1597∼1616 cm^{-1} shows hydrogen-bonded C=O, respectively (Ref 39). The absorbance peak at 1500∼1535 cm^{-1} is due to the aromatic ring, while the peak around 1225∼1241 cm^{-1} indicates the NHCOO group of newly synthesized products, respectively (Ref 40). The characteristic stretching absorbance band of C-O-C corresponds to around 1078∼1088 cm^{-1} which confirms linkage between OH and NCO group which provides strong evidence of PU synthesis (Ref 41, 42).

The peaks around 3335-3400cm^{-1} in all samples indicate that as FMWCNTs concentration increases, the peak becomes less broad due to greater FMWCNT-PU interaction. As filler content increases, the N-H characteristic peak becomes less broad as Fig. 3 represents. It confirms the synthesis of PU-nanocomposites through the grafting of FMWCNTs in the polymer matrix and its proper fabrication in the PU polymer matrix.

3.2 XRD Analysis

The fabrication of FMWCNTs was firstly investigated by the x-ray diffraction method, which also informs about the crystallographic properties of TPUs and their nanocomposites. Fig. 4 reveals the WAXS of pristine-PU and its nanocomposites with different loading amounts of FMWCNTs nanofiller. The PU-nanocomposites did not show peak 2θ=26° due to orderly arrangement and uniform dispersion of FMWCNTs carbon concentric cylinders-based filler and better interfacial interaction. The diffraction peak around 2θ=43° is because of carbon/graphitic planes and trapped catalyst inside FMWCNTs during their functionalization process (Ref 43-45). The typical diffraction peak around 2θ=20° represents the thermoplastic hard crystalline domains for filler filled and neat-PU. Amorphous regions display large scattered areas and the addition of FMWCNTs narrows the TPUs crystalline peak of hard domains, which indicates an increase in the degree of crystallinity. The small diffraction peak around 2θ=43° attributes to the higher concentration of FMWCNTs structures in nanocomposites and Vander wall forces and π-π interactions and it also suggests some re-aggregation in PU matrix. The additions of dual-FMWCNTs assist the non-crystalline part of hard domains to regulate its structure into the crystalline phase (Ref 46).

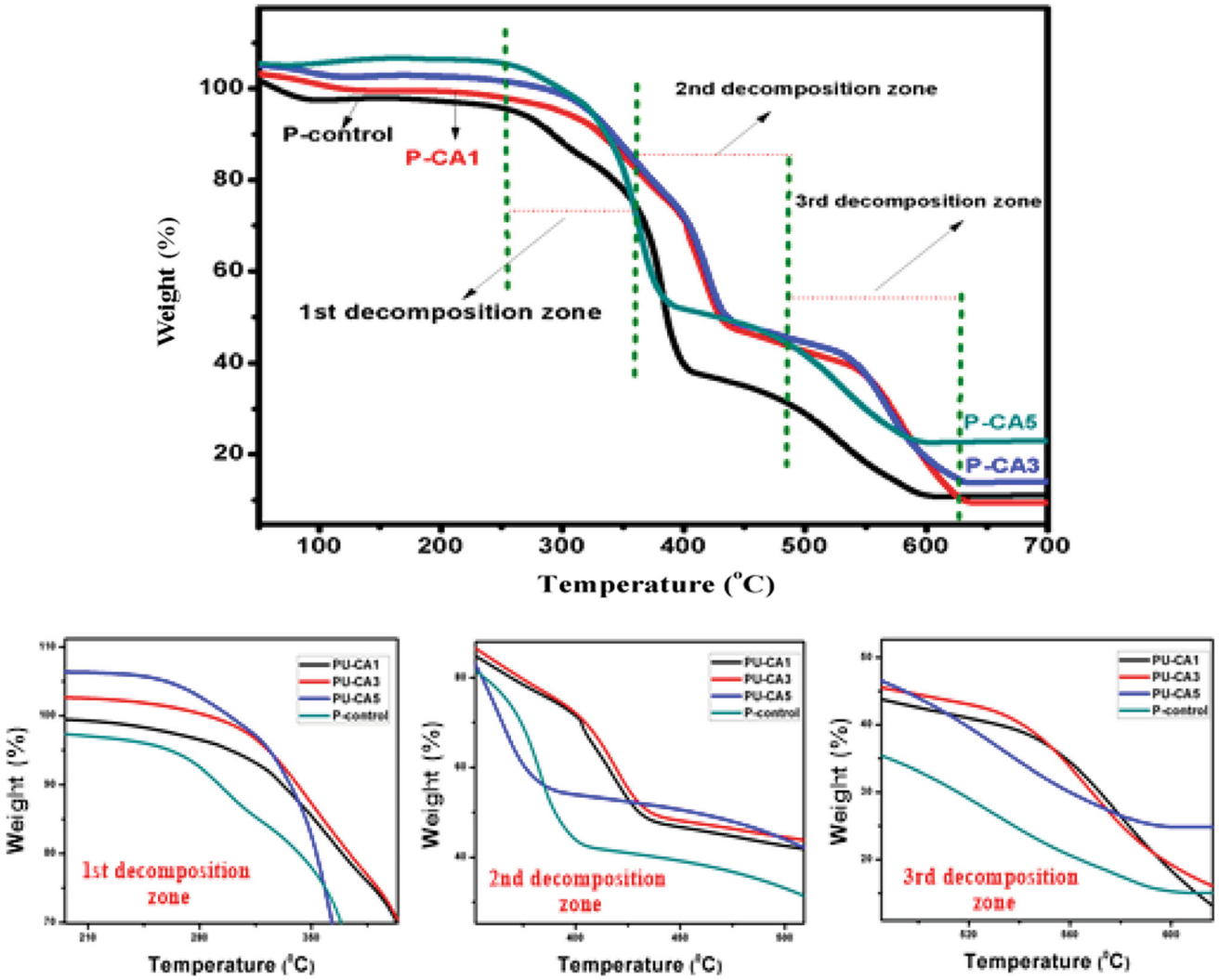

Fig. 5 TGA micrograph of selected samples (P-control, P-CA1, P-CA3, and P-CA5), (a): complete thermal decomposition of selected samples, (b): represents first decomposition zone, (c): second decomposition zone, (d): third decomposition zone during thermal decomposition

3.3 TGA Analysis

The thermal stability pattern of pristine-PU and its nanocomposites with a mixture of dual-functionalized MWCNTs under (N_2) inert atmosphere is illustrated in Fig. 5. Figure 5A presents percentage (%) weight loss as temperature increased up to 750 °C called TGA curves. Similarly, Fig. 6 depicts a derivative of %weight loss with increasing temperature called DTG curves. The key determining parameters from Fig. 5 and Fig. 6 are presented in Table 2. The $Td_{10\%}$, $Td_{50\%}$, $Td_{70\%}$ and $Td_{100\%}$ are at temperature where 10%, 50%, 70% and 100% weight loss have been identified, respectively. Similarly, T_{max} is the temperature where the maximum loss in mass takes place in the DTGA curve. (Table 2)

Three main degradation stages are evident from TG/DTG data. In nanocomposites, the %age decomposition values and the temperature maximum weight loss have been shifted toward higher values as compared to the pristine-PU, for nanocomposites having a mixture of dual-functionalized MWCNTs as Table 2 data present. The $Td_{10\%}$, $Td_{50\%}$, and $Td_{70\%}$ of pristine-PU are 288,386 and 487 °C, respectively, while for nanocomposites having 0.05 g of FMWCNTs mixture, the thermal decomposition values stand at 327, 429, and 571 °C. By increasing more amount of hybrid functionalized filler up to 0.1 g, the percentage weight loss was observed at 338, 438, and 568 °C, respectively.

The results indicate the positive effect of FMWCNTs mixture on relative thermal stabilities in PU-nanocomposites with increase loading amount. The efficient enhancement in relative thermal stabilities of composites is related to high thermal heat conductivity and diffusivity of FMWCNTs as compared to pristine-PU. Dual-functionalized MWCNTs can delay the thermal degradation phenomenon by serving as a barrier against underlying PU matrix degradation product fast removal. We also suggest due to amino-functionalized MWCNTs, strong chemical interaction is developed and acid-functionalized MWCNTs physical interaction was established. The strong interfacial interaction was developed by uniform dispersion and grafting of amino-functionalized MWCNTs in the polymer matrix because uniform dispersion provides an efficient platform for chemical and physical interaction between nanofiller and polymer matrix. It significantly reduces PUs and FMWCNTs thermal boundary resistance and helps the inefficient transfer of heat from the TPUs matrix and FMWCNTs

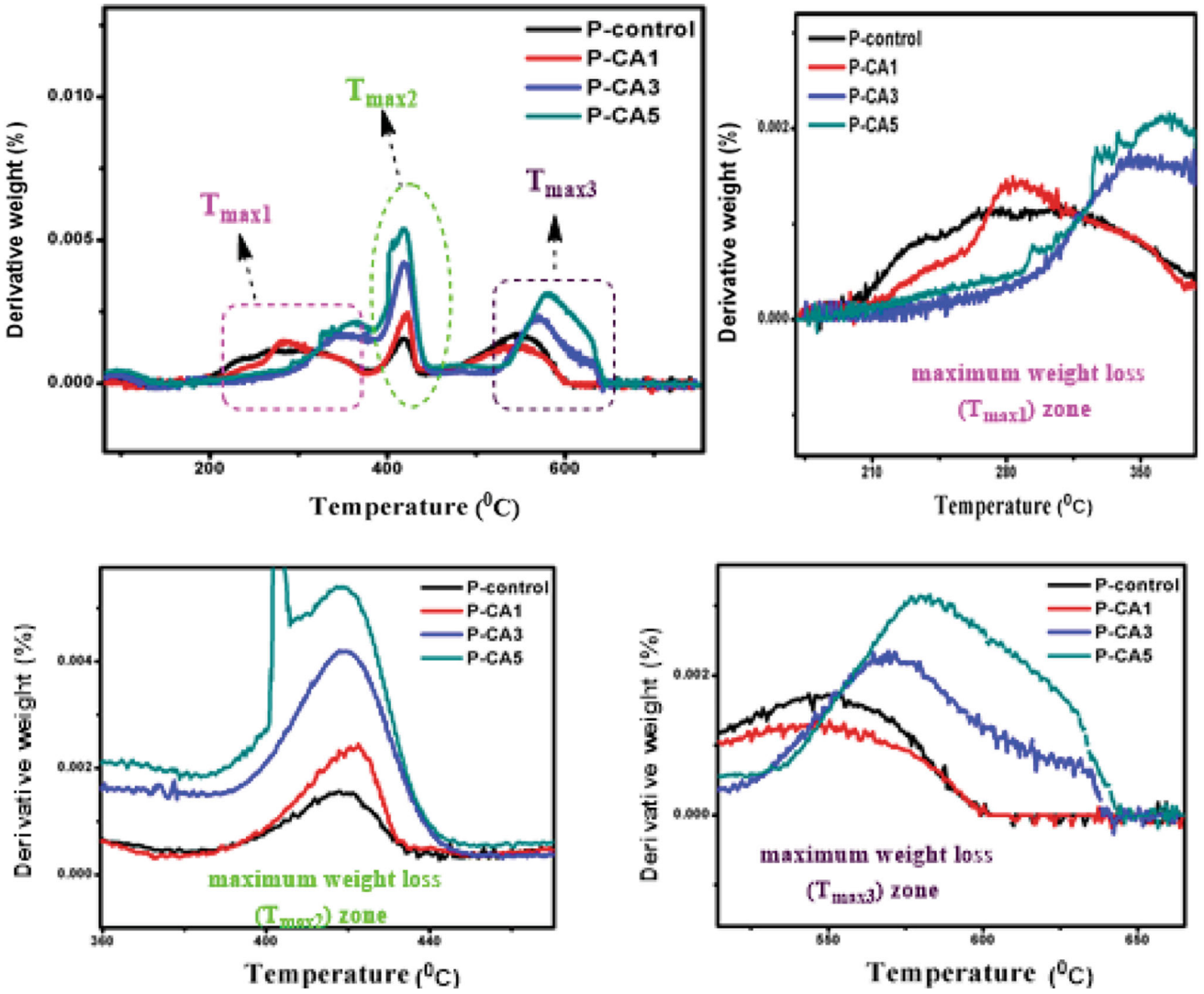

Fig. 6 DTG micrograph of selected samples (P-control, P-CA1, P-CA3, and P-CA5), (a): complete DTG curve of selected samples, (b): represents first maximum thermal decomposition zone, (c): second maximum decomposition zone, (d): third maximum decomposition zone during thermal decomposition

filler. This process facilitates smooth allotment in nanocomposite samples by greatly reducing the occurrence of hot spots.

The low loading amount of FMWCNTs can assist in lowering the glass transition temperature (Tg) for nanocomposites. More the chemical and physical interaction between nanofiller and polymer matrix in case of dual-functionalized filler (amino and acid functionalized) more will be the chemical and physical interaction, which helps to enhance thermal stabilities and reduces thermal decomposition by acting as a barrier. The sufficient incorporation and proper fabrication of FMWCNTs can also limit the mobility of the polymer chain which also causes enhancement in tensile and shape recovery properties (Ref 47, 48). More char residue is also evident for FMWCNTs loading amount increases as compared to pristine-PU, which also serves as a barrier for volatile products during decomposition. The char residue for the sample was observed 11.2, 11.6, 14.1, and 23%, respectively, as the loading amount of dual-functionalized filler increases as discussed in Table 2.

3.4 SEM Analysis

The SEM micrograph in Fig. 7 is observed under SEM for neat-PU and its nanocomposites with dual-FMWCNTs. Relatively very smooth surface morphology was observed for pristine-PU in (Fig. A). In the case of dual-FMWCNTs loading 0.01 g, some MWCNTs embedded nanotubes are visible on the surface due to better interfacial interaction of grafted FMCNTs and properly fabricated FMWCNTs in the TPUs matrix. Some aggregates are also visible in the case of 0.05g and 0.1 g loading amount of dual-FMWCNTs filler (Fig. 7 C&D) with proper fabrication and uniform dispersion. Furthermore, FMWCNTs enrich aggregates are still evident as the concentration of filler increases. Apart from little aggregates and enrich FMWCNTs domains, the dual-FMWCNTs filler presents good dispersion of dual-FMWCNTs as can be seen in (Fig. 7 B-E). In SEM micrograph, phase separation is evident in most of the cases between both phases. The theory of uniform dispersion of dual-FMWCNTs in the polymer matrix is also supported by some obvious white spots. As the loading amount

Table 2 TG- DTG analysis of blend nanocomposite samples (PU-5sim, PU-5com, PU-5C1, PU-5C2, and PU-5C3)

Sample code	T_d 50% , ˚C	T_d 70% , ˚C	$T_{max\ 1}$, ˚C	$T_{max\ 2}$, ˚C	$T_{max\ 3}$, ˚C	Char residue % over 700 , ˚C
P-control	386	487	276	418	546	11.2
P-CA1	429	568	296	422	556	11.6
P-CA3	435	571	349	428	575	14.1
P-CA5	422	551	361	436	583	22.8

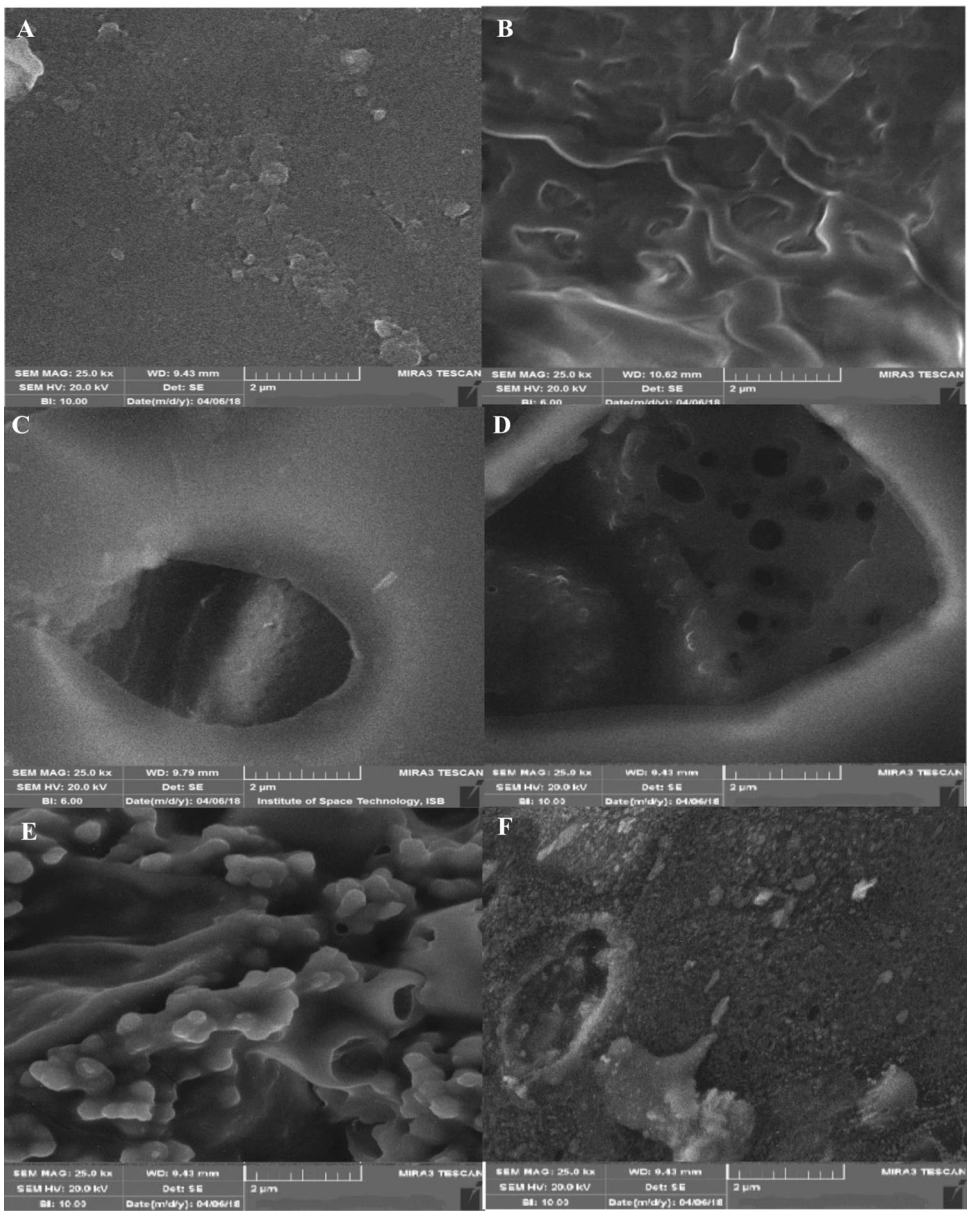

Fig. 7 SEM micrograph of samples at a different resolution, (a): P-control, (b): P-CA1, (c): P-CA2, (d): P-CA3, (e): P-CA4, and (f): P-CA5

of FMWCNTs increases, a few polymer-coated FMWCNTs are visible in the SEM micrograph.

Quite a few particles of the hard-phase were also observed dispersed and encapsulated in the PU matrix. A few of the crystallites can be observed in micrographs of different sizes and shapes due to the rigid domains of the PU matrix. With a low loading amount, FMWCNTs are not visible but as the loading amount increases, some obvious white spots become visible which favors the idea of properly grafted and fabrication of FMWCNTs in polymer matrix by generating both chemical and physical interaction. However, some porosity is also evident due to less grafting and not uniform dispersion of FMWCNTs in the polymer matrix.

As the loading amount of FMWCNTs increased up to 0.5g, the aggregation is visible due to the formation of globules. The rough and dispersed surface can be seen in (Fig. 7F). As the

concentration of FMWCNTs increases from a certain level, it starts restacking and form a rough surface with evident aggregation on the surface which effect on tensile and shape recovery properties.

The main mechanism suggested for uniform dispersion state in TPUs-nanocomposites is that twisted and long MWCNTs can lodge between multi-layers to minimize multi-layer restacking. The second most probable phenomenon involved in uniform dispersion is chemical (grafting of amino-FMWCNTs) and physical (acid-FMWCNTs) interaction with PUs matrix. The strong physical and chemical interaction between nanofiller and polymer can help in the proper uniform fabrication of nanofiller in polymer by avoiding re-aggregation and agglomeration. The physically and chemically interconnected structures due to dual-FMWCNTs help to enhance proper fabrication by generating interconnected networks. The dual-FMWCNTs prevent FMWCNTs from restacking while also favoring uniform dispersion in the polymer matrix. These physically and chemically grafted interconnected structures of dual-FMWCNTs and PUs matrix are known as hybrid functional filler networks.

CNTs form stronger three-dimensional networks due to their strong three-dimensional networks allowing for appropriate fabrication. We anticipate that the nanocomposite will have improved mechanical, thermal, and shape recovery properties as a result of these interactions. Similarly, non-covalent interaction has been found indispensable for the shape recovery performance of PUs.

3.5 Tensile Strength

A small loading amount of FMWCNTs can help to increase storage modulus and tensile properties of TPUs nanocomposites, also it can cause a decrease in glass transition temperature. Stronger will be the interfacial interaction larger will be storage modulus by limiting polymer chain segment motion. The chemical interaction (grafting) and physical cross-linking between FMWCNTs and TPUs play a vital role to predict the mechanical properties of the nanocomposites.

In particular research, the loading amount of 0.3 g of dual-FMWCNTs mixture showed excellent mechanical properties. Table 3 presents the tensile properties of pristine-PU and its nanocomposites. Increment in tensile properties and strength of nanocomposites with increasing loading amount of filler is rapid and prominent. The observed tensile strength of pristine-PU was 32.17 MPa, while by incorporation of 0.01 g of dual-FMWCNTs, the observed enhancement was 47.98 MPa. Similarly, by adding 0.3 g of FMWCNTs, the maximum tensile strength of 62.13 MPA was achieved as shown in Fig. 8. More amount of filler causes a decrease in tensile strength due to re-aggregation and globules formation after that limit, as seen in SEM micrographs.

We suggest that significant enhancement in mechanical properties is achieved due to sufficient interfacial interaction by grafting of amino-FMWCNTs and physical interaction of acid-FMWCNTs with TPUs, which causes a high degree of load transfer. Another important factor of the significant improvement in tensile properties is FMWCNT's higher modulus due to the higher volume fraction in the PUs matrix. The dual-FMWCNTs-based TPUs fracture strain values decreased by filler restacking and agglomeration, filler causes imperfection and voids which result in local stress concentration (Ref 49, 50).

The strength of nanocomposites' tensile properties is dependent on the chemical and physical interaction of nanofiller with polymer chain and distribution pattern of both phases. The nanofiller distribution effect is apparent in the tensile properties of the nanocomposites. The tensile data trends for all nanocomposite samples reveal that tensile properties have sufficient enhancement as dual-FMWCNTS loading amount increases. A sudden increase in tensile properties is evident when 0.01g of dual-FMWCNTs mixture was added. It is clearly due to chemical interaction formed between the thermoplastic-PU chain and amino-FMWCNTs (called FMWCNTs grafting), while acid-FMWCNTs form physically cross-linked networks which also play a vital role in tensile properties enhancement. Due to efficient chemical and physical cross-linking, proper fabrication enhancement in tensile properties is evident up to 0.3g of dual-FMWCNTs loading concentration. But as the concentration of filler increases up to 0.5g, it causes voids and defects due to restacking and re-aggregation of nanofiller in polymer matrix by forming globules and causes a decrease in tensile strength. Another suggested reason for the decrease in tensile strength is less interaction between FMWCNTs adsorption over PU chain surface.

According to mixture law addition of functionalized filler imparts positive deviation in mechanical strength. Until low loading amounts up to 3% sufficient enhancement in mechanical strength is evident due to better dispersion of CNTs in matrix chain by generating filler-polymer networks which help in efficient load transfer. The MWCNTs tortious nature and conductance help to enhance mechanical properties by generating physical and chemical interaction and networks with polymer chains. Functionalized filler such as amino and acidic functionalized MWCNTs plays a vital role by generating these networks to increase mechanical strength. More addition of functionalization leads toward the aggregation in a polymer matrix which effectively decreases the mechanical strength of the nanocomposite due to microcrack generation. Uniform dispersion even at a low loading amount of filler content can

Table 3 Tensile test data of neat-PU, PU-com, and blends with varying FMWCNTs ratios

Samples code	Tensile strength, MPa	Load at break, N	Extension at break, mm	Break elongation, %
P-control	32.17±1.2	91.84±4.3	0.85±0.3	4.10± 0.9
P-CA1	47.48±2.1	116.01±5.7	1.09±0.7	5.28± 0.11
P-CA2	48.90±2.4	117.09±5.4	1.13±0.2	5.34 ±0.17
P-CA3	50.81±1.9	138.61±4.3	1.24±0.7	5.9 ± 0.15
P-CA4	62.13±3.1	211.29 ±4.7	1.34±0.9	6.44 ± 0.2
P-CA5	40.83±1.8	107.25±4.2	0.99±0.2	4.76 ±0.17

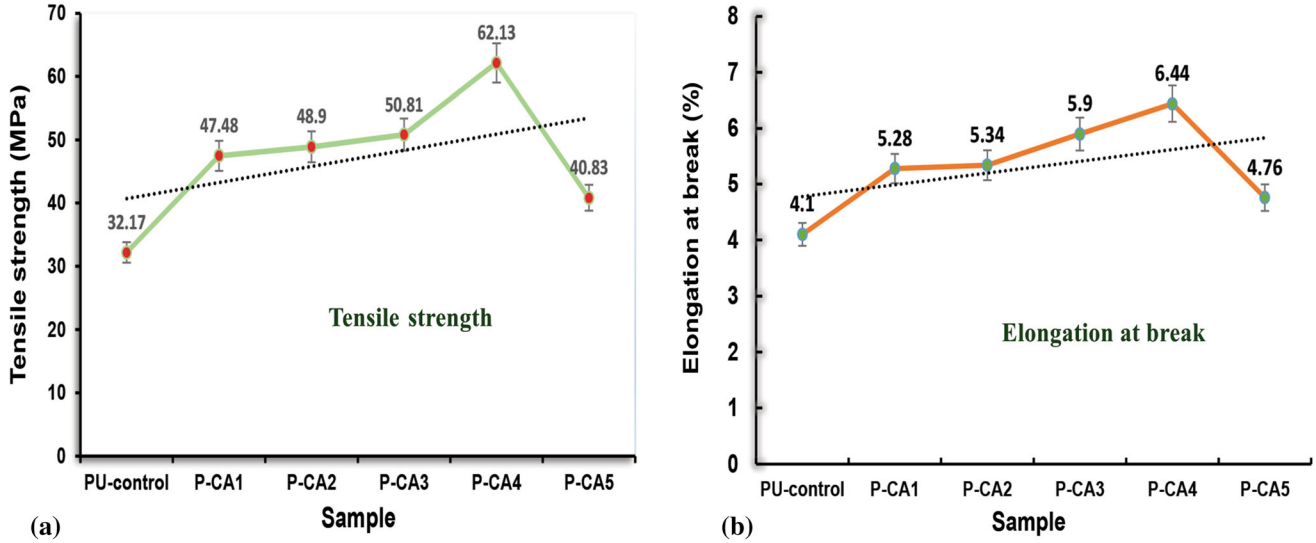

Fig. 8 Tensile values of all selected samples (a): tensile strength, (b): break elongation

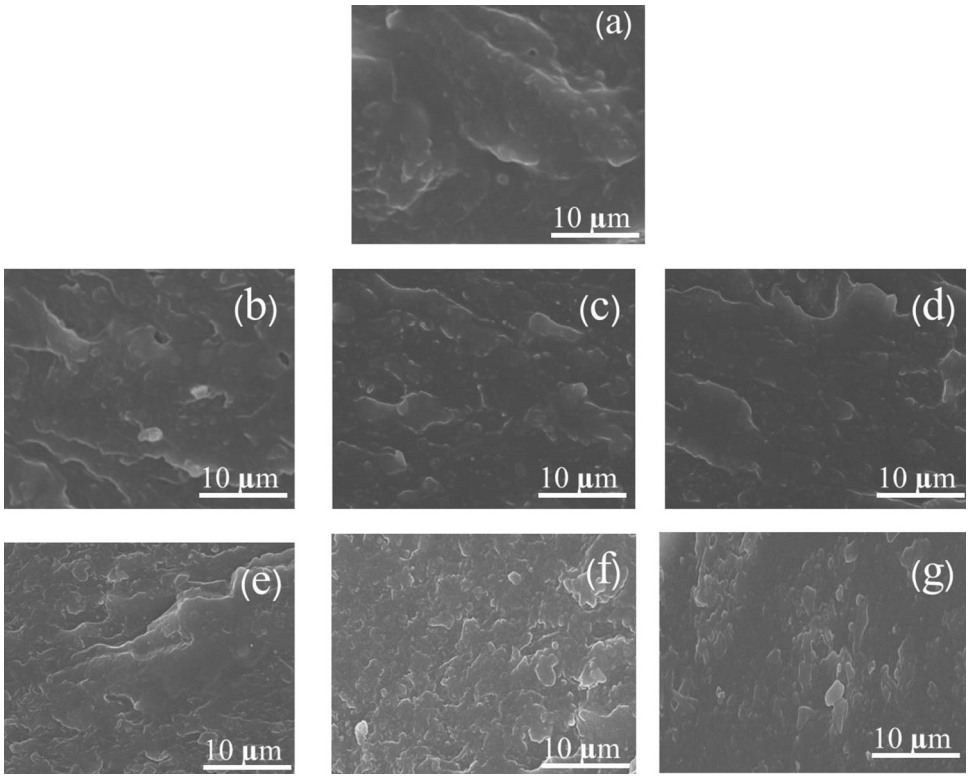

Fig. 9 SEM micrograph of samples after tensile testing, (a): P-control, (b): P-CA1, (c): P-CA2, (d): P-CA3, (e): P-CA4, and (f): P-CA5

cause sufficient enhancement in mechanical strength and also thermal conductivities of polymer nanocomposites which effectively help in shape recovery and repeatability.

The SEM fractography on tension test composite specimens was conducted and it shows uniform dispersion of MWCNTs without any obvious agglomerates. This also depicts that the MWCNTs have formed strong interaction with PU and possess excellent interfacial compatibility within PU matrix (Ref 51).

3.6 Shape Memory Behavior

Thermal triggering of shape recovery is observed through indirect heating by folding sample in U-shape at high temperature, followed by successive cooling at an ambient temperature around 20^0C o attain temporarily deformed shape. The complete phenomenon is illustrated in Fig. 2. A prompt response was observed for all the samples under heat. The shape recovery time of pristine-PU and its nanocomposites was

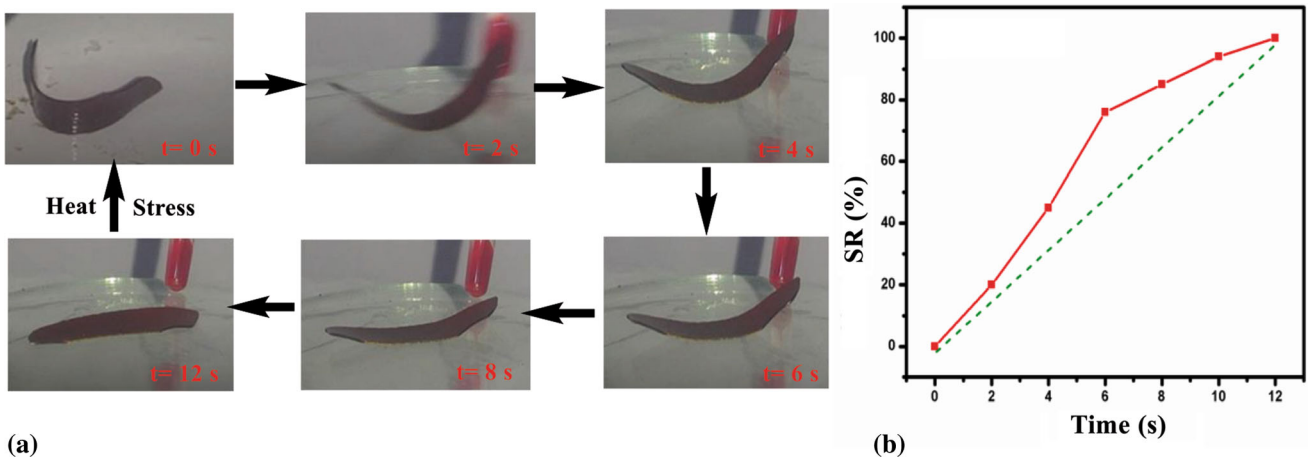

Fig. 10 (a): Thermally induced shape memory phenomenon of bPristine-PU (b): % shape recovery graph

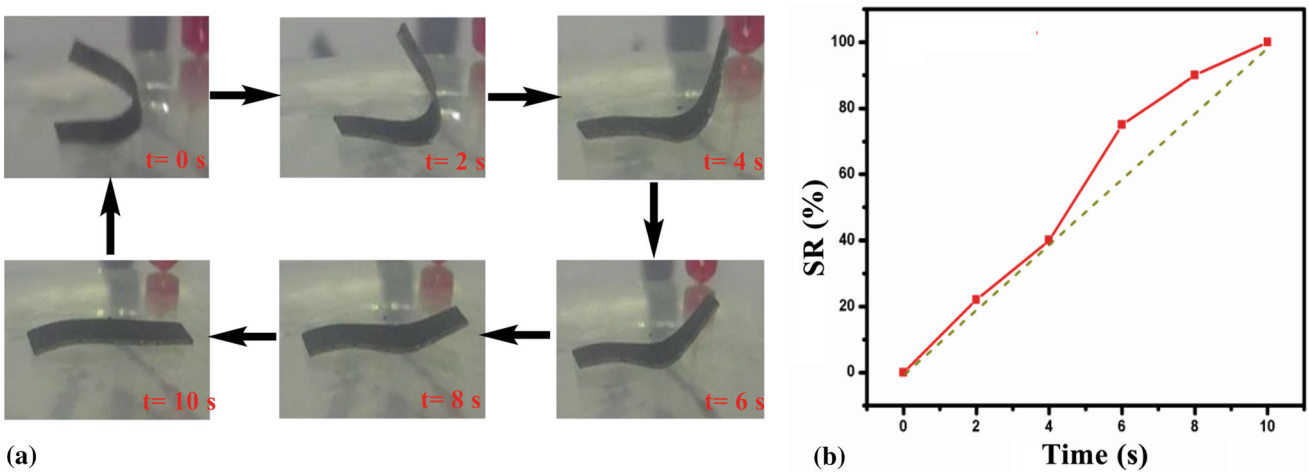

Fig. 11 (a): Thermally triggered shape memory phenomenon of P-CA1 (b): % shape recovery graph

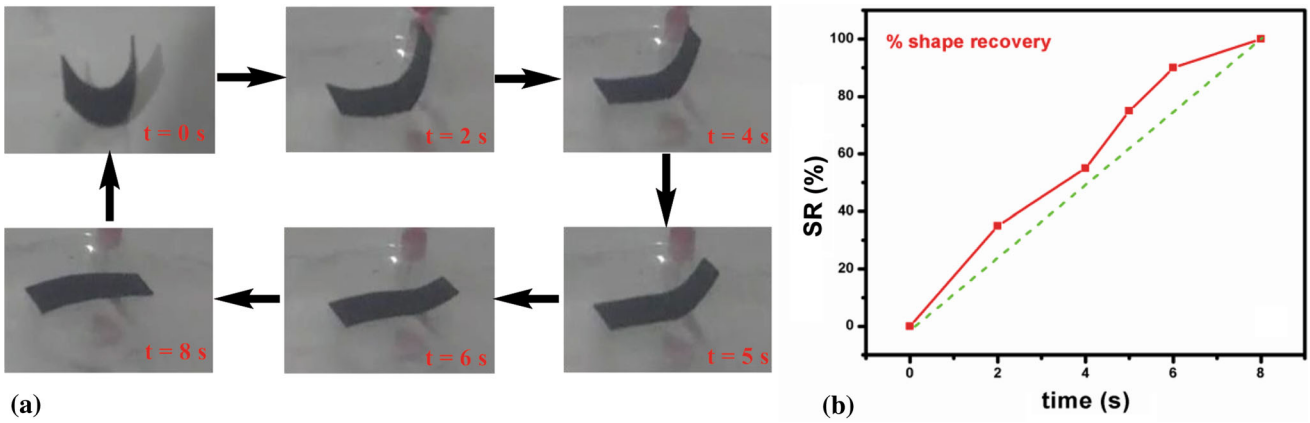

Fig. 12 (a): Thermally triggered shape memory phenomenon of P-CA4 (b): % shape recovery graph

recorded and compared, almost 100% shape recovery was observed for the entire samples concerning time (Ref 52).

Pristine-PU complete recovery response was observed after 12 seconds (s) to its original shape from deformed temporary shape as presented in Fig. 10. Nanocomposite with 0.01g loading of dual-FMWCNTs mixture, almost 100% shape recovery, was observed after 10s of consecutive heating. After that complete recovery, no other change in shape was evident

even after 2 minutes of heating as depicted in Fig. 11. Similarly using more quantities of dual-FMWCNTs filler up to 0.3g, the shape recovery time was reduced to 8s as shown in Fig. 11 A (supplementary videos are attached). The presented results for all the samples show 100% shape recovery in a very small interval of time which is an excellent achievement for these kinds of polymer materials.

Dual-FMWCNTs incorporation in PU matrix results in a noticeable increment in shape recovery. The fact is accredited to the formation of chemical interaction (grafting) and physical interlinking pathways over a nanofiller surface that helps to strengthen the polymer network due to better interfacial interaction. Thermal, electrical conductivity, and tensile properties are critical parameters to attain high-performance shape recovery PU and its nanocomposites.

PU consists of alternating hard and soft segment domains, heating above glass transition temperature (Tg) alternation in switchable domains takes place and polymer become rubbery from the brittle state. A particular condition by applying physical stress polymer can be molded into the desired temporary shape without any fracture or weak point. Sufficient cooling in an ambient environment helps in temporary shape fixation. Soft domains play a vital role in deformation because it provides a spring-like architecture to PU matrix and also helps to store deformation mechanical energy. The reason for taking a larger time for a complete recovery by pristine-PU is the poor electrical and thermal conductivity of PU, while due to excellent thermal capabilities and tortuous nature, CNTs can help in uniform conduction of heat and electricity in the sample (Ref 52). Dual-FMWCNTs form strong physical and chemical interaction and act as an excellent material for thermal conduction. Due to excellent conductive properties, PU-nanocomposites show a prompt response to heat and more enhanced and reduced time shape recovery can be observed.

Uniform dispersion has a key role in predicting tensile, thermal, and shape recovery properties because better dispersion better will be electrical and thermal conductivities. In some cases, restacking and agglomeration can disturb the uniform dispersion of filler in the PU matrix as can be seen in Fig. 7F of the SEM micrograph. Agglomerates have sufficient effect to reduce tensile, thermal, and shape recovery properties of the PU.

4. Conclusion

Controlling hard and soft segment content results in an excellent system with excellent enhanced mechanical properties can be achieved. The following conclusions can be drawn from the experimental data. Firstly, dual-FMWCNTs provide efficient dispersion by forming physical and chemical interactions with the PU chain. Secondly, efficient dispersion of MWCNTs by strong (physical and chemical) interlinking is intended to enhance mechanical, thermal, and shape recovery properties of the nanocomposites. By generating both physical and chemical interactions of nanofiller with polymer matrix stress-bearing capacity, mechanical, de-shaping, and shape recovery can be tailored. Efficient dispersion of filler by grafting different groups at nanofiller can significantly impact thermal stabilities, tensile strength, and efficient shape recovery in very little time. Almost 100% shape recovery of the prepared sample was achieved in less than 10s due to excellent thermal conductivities of PU-nanocomposites due to excellent dual-FMWCNTs cross-linking in the polymer chain. Due to efficient dispersion and cross-linking by the physical and chemical interaction of nanofiller, an abrupt increase in tensile strength is also evident from previously reported materials.

Acknowledgments

This funding is supported by the higher education commission (Ref. No. 527/IPFP-II(Batch-I)/SRGP/NAHE/HEC/2020/275). We thank you for the facility support of the Characterization at the National Center for Physics Quaid-i-Azam University Islamabad and institute of space technology Islamabad Pakistan.

Conflict of interest

The authors declare no conflict of interest.

References

1. F. Wang, R. Zhang, A. Lin, R. Chen, Q. Wu, T. Chen and P. Sun, Molecular Origin of the Shape Memory Properties of Heat-Shrink Crosslinked Polymers as Revealed by Solid-State NMR, *Polymer*, 2016, **107**, p 61–70.
2. A. Pinho, C. Buga and A. Piedade, The Chemistry Behind 4D Printing, *Appl. Mater. Today*, 2020, **19**, p 100611.
3. S. Miao, N. Castro, M. Nowicki, L. Xia, H. Cui, X. Zhou, W. Zhu, S.-J. Lee, K. Sarkar and G. Vozzi, 4D Printing of Polymeric Materials for Tissue and Organ Regeneration, *Mater. Today.*, 2017, **20**, p 577–591.
4. W. Miao, W. Zou, Y. Luo, N. Zheng, Q. Zhao and T. Xie, Structural Tuning of Polycaprolactone Based Thermadapt Shape Memory Polymer, *Polym. Chem.*, 2020, **11**, p 1369–1374.
5. C. Zeng, H. Seino, J. Ren and N. Yoshie, Polymers with Multishape Memory Controlled by Local Glass Transition Temperature, *ACS Appl. Mater. Interfac.*, 2014, **6**, p 2753–2758.
6. A. Bruni, F.G. Serra, A. Deregibus and T. Castroflorio, Shape-Memory Polymers in Dentistry: Systematic Review and Patent Landscape Report, *Materials*, 2019, **12**, p 2216.
7. Z. Liu, X. Lan, W. Bian, L. Liu, Q. Li, Y. Liu, J. Leng, Design, Material Properties and Performances of a Smart Hinge Based on Shape Memory Polymer Composites, *Comp. Part B: Engg.*,2020, 108056
8. A. Ben Abdallah, F. Gamaoun, A. Kallel and A. Tcharkhtchi, Molecular Weight Influence on Shape Memory Effect of Shape Memory Polymer Blend (Poly (Caprolactone)/Styrene-Butadiene-Styrene), *J. Appl. Polym. Sci.*, 2020, **138**, p 49761.
9. S. Shree, M. Dowds, A. Kuntze, Y.K. Mishra, A. Staubitz and R. Adelung, Self-Reporting Mechanochromic Coating: A Glassfiber Reinforced Polymer Composite that Predicts Impact Induced Damage, *Mater. Hori.*, 2020, **7**, p 598–604.
10. J. Marx, S. Roth, A. Brouschkin, D. Smazna, Y.K. Mishra, K. Schulte, R. Adelung and B. Fiedler, Tailored Crystalline Width and Wall Thickness of an Annealed 3D Carbon Foam Composites and Their Mechanical Properties, *Carbon*, 2019, **142**, p 60–67.
11. S.K. Srivastava and Y.K. Mishra, Nanocarbon Reinforced Rubber Nanocomposites: Detailed Insights About Mechanical, Dynamical Mechanical Properties, Payne, and Mullin Effects, *Nanomater.*, 2018, **8**, p 945.
12. Q. Zhao, H.J. Qi and T. Xie, Recent Progress in Shape Memory Polymer: New Behavior, Enabling Materials, and Mechanistic Understanding, *Prog. Polym. Sci.*, 2015, **49**, p 79–120.
13. J. Leng, X. Lan, Y. Liu and S. Du, Shape-Memory Polymers and Their Composites: Stimulus Methods and Applications, *Prog. Polym. Sci*, 2011, **56**, p p1077-1135.
14. Y. Liu, H. Du, L. Liu and J. Leng, Shape Memory Polymers and Their Composites in Aerospace Applications: A Review, *Smart Mater. Struct.*, 2014, **23**, p 023001.
15. M. Ebara, Y. Kotsuchibashi, K. Uto, T. Aoyagi, Y.-J. Kim, R. Narain, N. Idota and J.M. Hoffman, *Shape-Memory Materials*, Springer, Smart Biomaterialsed., 2014, p 285–373

16. P.T. Mather, X. Luo and I.A. Rousseau, Shape Memory Polymer Research, *Annu. Rev. Mater. Res.*, 2009, **39**, p 445–471.
17. A. Pandey, G. Singh, S. Singh, K. Jha, C. Prakash, 3D Printed Biodegradable Functional Temperature-Stimuli Shape Memory Polymer for Customized Scaffoldings, *J. Mechan. Behav. Biomed. Mater.*,2020. 103781
18. A. Khan, N. Ahmed, M. Rabnawaz, Covalent Adaptable Network and Self-Healing Materials: Current Trends and Future Prospects in Sustainability, *Polym.*, 2020,p 2027
19. W. Xu, M. Xiao, L. Yuan, J. Zhang and Z. Hou, Preparation, Physicochemical Properties and Hemocompatibility of Biodegradable Chitooligosaccharide-Based Polyurethane, *Polymer*, 2018, **10**, p 580.
20. F. Zia, K.M. Zia, M. Zuber, H.B. Ahmad and M. Muneer, Glucomannan Based Polyurethanes: A Critical Short Review of Recent Advances and Future Perspectives, *Inter. J. Biolog. Macromole.*, 2016, **87**, p 229–236.
21. B. Han, S. Sharma, T.A. Nguyen, L. Li, K.S. Bhat, Fiber-Reinforced Nanocomposites: Fundamentals and Applications, Elsevier, 2020
22. U. Arif, S. Haider, A. Haider, N. Khan, A.A. Alghyamah, N. Jamila, M.I. Khan, W.A. Almasry and I.-K. Kang, Biocompatible Polymers and their Potential Biomedical Applications: A Review, *Current Pharma. Des.*, 2019, **25**, p 3608–3619.
23. M. Irfan and M. Seiler, Encapsulation Using Hyperbranched Polymers: From Research and Technologies to Emerging Applications, *Indust. Engg. Chem. Res.*, 2010, **2010**(49), p 1169–1196.
24. S. Ahmed, Y. Cai, M. Ali, S. Khanal and S. Xu, Preparation and Performance of Nanoparticle-Reinforced Chitosan Proton-Exchange Membranes for Fuel-Cell Applications, *J. Appl. Polym. Sci.*, 2019, **136**, p 46904.
25. S. Ahmed, Y. Cai, M. Ali, S. Khannal and S. Xu, Preparation and Properties of Alkyl Benzene Sulfonic Acid Coated Boehmite/Chitosan Nanocomposite Membranes with Enhanced Proton Conductivity for Proton Exchange Membrane Fuel Cells, *Mater. Exp.*, 2019, **9**, p 42–50.
26. A.P. Kishan, T. Wilems, S. Mohiuddin and E.M. Cosgriff-Hernandez, Synthesis and Characterization of Plug-and-Play Polyurethane Urea Elastomers as Biodegradable Matrixes for Tissue Engineering Applications, *ACS Biomat. Sci. & Engg.*, 2017, **3**, p 3493–3502.
27. C. Christenson, M. Harthcock, M. Meadows, H. Spell, W. Howard, M. Creswick, R. Guerra and R. Turner, Model MDI/Butanediol Polyurethanes: Molecular Structure, Morphology, Physical and Mechanical Properties, *J. Polym. Sci. Part B: Polym. Phys.*, 1986, **24**, p 1401–1439.
28. T. Pretsch, I. Jakob and W. Müller, Hydrolytic Degradation and Functional Stability of a Segmented Shape Memory Poly (Ester Urethane), *Polym. Degr. Stab.*, 2009, **2009**(94), p 61–73.
29. S. Ahmed, M. Ali, Y. Cai, Y. Lu, Z. Ahmad, S. Khannal and S. Xu, Novel Sulfonated Multi-Walled Carbon Nanotubes Filled Chitosan Composite Membrane for Fuel-Cell Applications, *J. Appl. Polym. Sci.*, 2019, **136**, p 47603.
30. M.A. Awotunde, A.O. Adegbenjo, O.O. Ayodele, A.M. Okoro, M.B. Shongwe and P.A. Olubambi, Reactive Synthesis of CNTs Reinforced Nickel Aluminide Composites by Spark Plasma Sintering, *Mater. Sci. Engg. A*, 2020, **796**, p 140070.
31. C.I. Idumah, I. Nwuzor, S.S. Odera, Recent Advancements in Self-Healing Polymeric Hydrogels, Shape Memory, and Stretchable Materials, *Inte. J. Polym. Mater. Polymeric Biomat.*, 2020. 1-26
32. C.I. Idumah, S. Odera, Recent Advancement in Self-Healing Graphene Polymer Nanocomposites, Shape Memory, and Coating Materials, *Polym.Plast. Tech. Mater.*,2020. 1-24
33. N. Ahmed, B. Niaz, S. Nauman and M.T. Javid, Functionalized Carbon Nanotubes Based Thermo-Responsive Shape Memory Blends with Enhanced Mechanical Properties for Potential Robotics Applications, *Iran. Polym. J.*, 2020, **30**, p 67–80.
34. E. Ciecierska, M. Jurczyk-Kowalska, P. Bazarnik, M. Gloc, M. Kulesza, M. Kowalski, S. Krauze and M. Lewandowska, Flammability, Mechanical Properties and Structure of Rigid Polyurethane Foams with Different Types of Carbon Reinforcing Materials, *Comp. Struct.*, 2016, **140**, p 67–76.
35. T. Subhani, M. Latif, I. Ahmad, S.A. Rakha, N. Ali and A.A. Khurram, Mechanical Performance of Epoxy Matrix Hybrid Nanocomposites Containing Carbon Nanotubes and Nanodiamonds, *Mater. Des.*, 2015, **87**, p 436–444.
36. M. Dong, Q. Li, H. Liu, C. Liu, E.K. Wujcik, Q. Shao, T. Ding, X. Mai, C. Shen and Z. Guo, Thermoplastic Polyurethane-Carbon Black Nanocomposite Coating: Fabrication and Solid Particle Erosion Resistance, *Polymer*, 2018, **158**, p 381–390.
37. A. Radhamani, H.C. Lau and S. Ramakrishna, Structural, Mechanical and Corrosion Properties of CNT-304 Stainless Steel Nanocomposites, *Progress in Natural Science: Mater. Inter.*, 2019, **29**, p 595–602.
38. N. Ahmed, A. Kausar and B. Muhammad, Shape Memory Properties of Electrically Conductive multi-Walled Carbon nanotube-Filled Polyurethane/Modified Polystyrene Blends, *J. Plast. Film & Sheet.*, 2016, **32**, p p272-292.
39. Z. Akram, A. Kausar and M. Siddiq, Review on Polymer/Carbon Nanotube Composite Focusing Polystyrene Microsphere and Polystyrene Microsphere/Modified CNT Composite: Preparation, Properties, and Significance, *Polym.-Plast. Tech. Engg.*, 2016, **55**, p 582–603.
40. G. Trovati, E.A. Sanches, S.C. Neto, Y.P. Mascarenhas and G.O. Chierice, Characterization of Polyurethane Resins by FTIR, TGA, and XRD, *J. Appl. Polym. Sci.*, 2010, **115**, p 263–268.
41. S. Ahmed, Y. Cai, M. Ali, S. Khannal, Z. Ahmad, Y. Lu, S. Wang and S. Xu, One-Step Phosphorylation Of Graphene Oxide for the Fabrication Of Nanocomposite Membranes with Enhanced Proton Conductivity for Fuel Cell Applications, *J. Mater. Sci. Mater. Elect.*, 2019, **30**, p 13056–13066.
42. Z. Jiang, K. Yuan, S. Li and W. Chow, Study of FTIR Spectra and Thermal Analysis of Polyurethane, *Guang pu xue yu guang pu fen xi= Guang pu*, 2006, **26**, p 624–628.
43. S. Ahmed, T. Arshad, A. Zada, A. Afzal, M. Khan, A. Hussain, M. Hassan, M. Ali and S. Xu, Preparation and Characterization of a Novel Sulfonated Titanium Oxide Incorporated Chitosan Nanocomposite Membranes for Fuel Cell Application, *Memb.*, 2021, **11**, p 450.
44. L. Bistričić, G. Baranović, M. Leskovac and E.G. Bajsić, Hydrogen Bonding and Mechanical Properties of thin Films of Polyether-Based Polyurethane–Silica Nanocomposites, *Europ. Polym. J.*, 2010, **46**, p 1975–1987.
45. M. Hassan, A. Afzal, M. Tariq and S. Ahmed, Synthesis of the Hyper-Branched Polyamides and their Effective Utilization in Adsorption and Equilibrium Isothermal Study for Cadmium ion Uptake, *J. Polym. Res.*, 2021, **28**, p 1–11.
46. K.M. Zia, M. Zuber, M. Barikani, A. Jabbar and M.K. Khosa, XRD Pattern of Chitin Based Polyurethane Bio-Nanocomposites, *Carbo. polym.*, 2010, **80**, p 539–543.
47. A. Hezma, I. Elashmawi, E. Abdelrazek, A. Rajeh and M. Kamal, Enhancement of the Thermal and Mechanical Properties of Polyurethane/Polyvinyl Chloride Blend by Loading Single Walled Carbon Nanotubes, *Progress Nat. Sci. Mater. Inter.*, 2017, **27**, p 338–343.
48. M. Raja, A. Shanmugharaj, S.H. Ryu and J. Subha, Influence of Metal Nanoparticle Decorated CNTs on Polyurethane Based Electro Active Shape Memory Nanocomposite Actators, *Mater. Chem. Phys.*, 2011, **129**, p 925–931.
49. T. Hosseini-Sianaki, H. Nazockdast, B. Salehnia and E. Nazockdast, Microphase Separation and Hard Domain Assembly in Thermoplastic Polyurethane/Multiwalled Carbon Nanotube Nanocomposites, *Polym. Engg. Sci.*, 2015, **55**, p 2163–2173.
50. P. Visakh and O.B. Nazarenko, *Thermal degradation of polymer blends, composites and nanocomposites, Thermal Degradation of Polymer Blends*, Springer, Composites and Nanocomposites., 2015, p 1–16
51. X. Ren, R. Zong, Y. Hu, S. Lo, A.A. Stec and T.R. Hull, Investigation of Thermal Decomposition of Polymer Nanocomposites with Different Char Residues, *Polym. Adv. Tech.*, 2015, **26**, p 1027–1033.
52. J. Jyoti, B.P. Singh, A.K. Arya and S. Dhakate, Dynamic Mechanical Properties of Multiwall Carbon Nanotube Reinforced ABS Composites and Their Correlation with Entanglement Density, Adhesion, Reinforcement and C Factor, *RSC adv.*, 2016, **6**, p 3997–4006.